

ADVANCED MATERIALS

Supporting Information

for *Adv. Mater.*, DOI: 10.1002/adma.201907267

**Metal–Organic Framework Nanoparticles Induce Pyroptosis in
Cells Controlled by the Extracellular pH**

*Evelyn Ploetz, Andreas Zimpel, Valentina Cauda, David
Bauer, Don C. Lamb, Christoph Haisch, Stefan Zahler,
Angelika M. Vollmar, Stefan Wuttke,* and Hanna Engelke**

Supporting Information

Metal–Organic Framework Nanoparticles Induce Pyroptosis in Cells Controlled by the Extracellular pH

Evelyn Ploetz,^{a-c,#} Andreas Zimpel,^{a,#} Valentina Cauda,^d David Bauer,^e Don C. Lamb,^{a-c} Christoph Haisch,^e Stefan Zahler,^f Angelika M. Vollmar,^f Stefan Wuttke,^{a,g,h,*} and Hanna Engelke,^{a,*}

^a *Department of Chemistry and Center for NanoScience (CeNS), Ludwig-Maximilians-Universität München, Butenandtstraße 11, 81377 Munich, Germany*

^b *Nanosystems Initiative Munich (NIM), Ludwig-Maximilians-Universität München, Butenandtstraße 5-13, 81377, Germany*

^c *Center for Integrated Protein Science Munich (CiPSM), Ludwig-Maximilians-Universität München, Butenandtstraße 5-13, 81377 Munich, Germany*

^d *Department of Applied Science and Technology, Politecnico di Torino, Corso Duca degli Abruzzi 24, 10129 Torino, Italy*

^e *Department of Chemistry, Chair of Analytical Chemistry, Technical University of Munich, Marchioninistraße 17, 81377 Munich, Germany*

^f *Department of Pharmacy, LMU Munich, Butenandtstraße 5, 81377 Munich, Germany*

^g *BCMaterials, Basque Center for Materials, UPV/EHU Science Park, 48940 Leioa, Spain*

^h *Ikerbasque, Basque Foundation for Science, 48013, Bilbao, Spain*

[#] *Shared first authors*

Corresponding authors: stefan.wuttke@cup.uni-muenchen.de / hanna.engelke@cup.uni-muenchen.de

Table of Contents

Table of Contents	S2
1. Methods and Characterization	S3
2. Experimental Section	S6
2.1. Chemicals.....	S6
2.2. Synthesis of MIL-100(Fe) nanoparticles.....	S6
2.3. Labeling of MIL-100(Fe) nanoparticles for fluorescence imaging.....	S6
2.4. Preparation of DOPC liposomes.....	S7
2.5. Preparation of Lip-MOF nanoparticles.....	S7
2.6. Preparation of HEPES buffered glucose (HBG), simulated body fluid (SBF) and artificial lysosomal fluid (ALF).....	S7
2.7. Cell culture.....	S7
2.8. Cell viability assay (MTT).....	S7
2.9. Calcein AM viability assay.....	S8
2.10. Determination of the iron uptake in 24 h.....	S9
2.11. Determination of uptake mechanisms by thermal endocytosis inhibition.....	S9
2.12. Determination of endocytosis mechanism by addition of endocytosis inhibitors.....	S9
2.13. Determination of MOF degradation kinetics.....	S9
2.14. Western Blot GSDMD.....	S10
2.15. IL-1 β ELISA.....	S10
2.16. Multivariate Raman data analysis.....	S10
3. Supplementary Figures	S13
4. Supplementary Tables	S35
5. References	S36

1. Methods and Characterization

X-ray diffraction (XRD): XRD was measured with the STOE transmission diffractometer system Stadi MP with Cu $K\alpha_1$ radiation ($\lambda = 1.54060 \text{ \AA}$) and a Ge(111) single crystal monochromator. Diffraction patterns were recorded with a DECTRIS solid state strip detector MYTHEN 1K in an omega-2-theta scan mode using a step size of 4.71° and a counting time of 80 s per step.

Dynamic light scattering (DLS) and zeta-potential measurements: DLS and zeta-potential measurements were carried out using a Malvern Zetasizer (Nano Series, Nano-ZS). For pH dependent zeta-potential measurements, the zetasizer was equipped with a Multi Purpose Titrator (MPT-2, Malvern Panalytical Ltd, Malvern, UK). 10 mL of an aqueous solution of nanoparticles (0.1 mg/mL) was set to pH 4 with HCl (0.1 M) and titrated stepwise (steps of 0.5) to pH 8 with NaOH (0.01 or 0.1 M).

Sorption measurements: Nitrogen sorption isotherms were measured at 77 K with a Quantachrome NOVA 4000e. Approximately 20 mg of nanoparticles was degassed at 150 °C in high vacuum for at least 12 h prior to the measurement. Evaluation of the sorption data was carried out using the ASiQwinTM software (Version 2.0, Quantachrome Instruments). Brunauer Emmett Teller (BET) surface areas were calculated using the linearized form of the BET equation. For all samples, the correlation coefficient was higher than 0.999. Adsorption isotherms were used to calculate the pore size distribution by employing quenched solid density functional theory (QSDFT, nitrogen at 77 K on carbon, cylindrical/spherical pores adsorption branch).

Infrared (IR) spectroscopy: IR spectroscopy was performed on an FT-IR spectrometer (Thermo Scientific, NICOLET 6700) in transmission mode. Transparent potassium bromide pellets (150 mg) served as the matrix for 1 mg of the testing substance.

UV-Vis spectroscopy: UV-Vis spectra were recorded using a Perkin-Elmer Lambda 1050 spectrometer equipped with a 150 mm integrating sphere.

Scanning electron microscopy (SEM): SEM measurements were carried out using a FEI HELIOS NANOLAB G3 UC microscope equipped with a field emission gun and operated at acceleration voltages between 2 and 20 kV. The nanoparticle suspension (30 μL , 1 mg/mL) was dropped on a carbon grid, placed on the SEM sample holder and was dried overnight.

High resolution transmission electron microscopy (HRTEM): High resolution TEM was performed using an FEI Titan Themis electron microscope equipped with an extreme field emission gun (X-FEG). A $4k \times 4k$ Ceta 16MTM camera detected bright field and high-resolution TEM images.

The samples were prepared by adding a droplet of the diluted ethanolic nanoparticle suspension on a carbon-coated copper grid followed by drying for a few minutes.

Confocal laser scanning microscopy (CLSM): High resolution live-cell microscopy was performed utilizing a spinning disk confocal microscope (Zeiss Observer SD with a Yokogawa CSU-X1 spinning disc unit) and a 63x objective at 37 °C and 5 % CO₂. For excitation, a 488 nm (lysosome-GFP) and 639 nm laser (Atto647N-loaded MOF) were used. Emission was filtered with a BP 525/50 and a LP 690 filter respectively. Cells were seeded into ibiTreat 8-well slides (ibidi) at a concentration of 5000 cells per well 24-72 h prior to imaging.

For lysosomal staining, CellLight lysosomes-GFP (BacMam 2.0, Thermofisher Scientific) was added to the cells 24 h after cell seeding and at least 24 h before imaging according to the supplier's protocol. Lip-MOF-ATTO647N nanoparticles (10 µL, c_{Stock}= 1 mg/mL) were added 24 h post seeding and microscopy was performed after 40 h of incubation without medium exchange. Lysosome-GFP was excited with 488 nm excitation light with an exposure time of 800 ms. ATTO647N was excited with 639 nm excitation light with an exposure time of 100 ms.

For lipid ROS detection, cells were incubated with Lip-MOF 24 h after seeding. Prior to imaging and 48 h after Lip-MOF incubation, 10 µM lipid ROS marker Bodipy-C11 was added according to the manufacturer's instructions. Bodipy-C11 was imaged using 488 nm and 561 nm excitation and BP 525/50 and BP 629/62 as emission filter, respectively, to observe the blue shift in fluorescence emission by Bodipy-C11 upon ROS generation.

Time-lapse imaging of calcein-loaded Lip-MOF was performed on an ImageXpress Micro XLS (Molecular Devices) widefield high-content microscope system. 5000 cells were seeded per well into a 96-well plate. 24 h after seeding, 20 µl of a 0.1 mg/mL solution of calcein-loaded Lip-MOF was added per well. 1 h after addition of Lip-MOF, cells were washed with medium and image acquisition was started using a 20x objective (super plan fluor ELWD DM, Nikon), a brightfield channel for cell imaging and a Semrock GFP filter block (AHF Analysentechnik; Germany) for imaging of the calcein-loaded Lip-MOF. Images were acquired every 15 mins over a time span of at least 72 h and cells were kept at 37 °C and 5 % CO₂ atmosphere. Recorded data was processed using ImageJ2 and Matlab2016b.

Raman microscopy: Hyper-spectral imaging was carried out using an inverted scanning Raman microscope (alpha300R, WITec GmbH, Ulm, Germany) equipped with a 532 nm CW laser source (Cobolt AB, Solna, Sweden) and 63x 1.2 NA water immersion objective (Zeiss W Plan-Apochromat). Excitation and detection paths are decoupled by a long-pass edge filter that blocks shorter wavelengths including Rayleigh scattering at 532 nm. Raman backscattered radiation was collected through the microscope objective and recorded via a lens-based spectrometer with CCD-camera (1600X200 pixel at -60 °C) with a spectral resolution of ~3.7 cm⁻¹ per pixel (Grating with 600 l/mm and blazed at 500 nm). For image acquisition, areas with 500 nm step-size were raster scanned while full Raman spectra

were recorded at each pixel of the image. The acquisition time per pixel was set to 150 ms with an excitation power of 5 mW at the sample. To characterize the cells on the confocal Raman microscope, HeLa cells were seeded on poly-lysine coated 35 mm wide glass bottom dishes (MatTek Corp. Ashland, USA, P35GC-0-14-C) and grown over night in DMEM either at pH 7.2 or 7.4. Before data acquisition, dishes were washed and filled with DMEM at the respective pH without phenol red.

Inductively Coupled Plasma Optical Emission Spectrometry (ICP-OES): Measurements were performed utilizing a radial view, Simultaneous ICP-OES (Vista RL, Varian, Mulgrave, Australia) equipped with a CCD detector. Samples were dissolved in HNO₃ conc. (69 % for trace analysis, Aristar®, VWR) and diluted to the appropriate iron concentration. Recorded data was evaluated using Excel and Origin9.0.

pH Measurements: All pH measurements were performed by a SevenEasy pH Meter (Mettler Toledo, Ohio, USA), which was calibrated by buffer solutions of pH 4.01, pH 7.00 and pH 9.21. For measurements of the media under cell culture conditions (37 °C, 5 % CO₂), the pH Meter was placed in a Galaxy® 14s Incubator (New Brunswick/Eppendorf AG, Germany).

2. Experimental section

2.1. Chemicals

Iron(III) chloride hexahydrate (Grüssing GmbH), iron(III) oxide (alpha-phase, nanopowder, 98%, Alfa Aesar), trimesic acid (BTC, Aldrich), 1,2-dioleoyl-*sn*-glycero-3-phosphocholine (Avanti Polar Lipids, Inc.; Alabama, USA), Dulbecco's Phosphate-Buffered Saline (DPBS, no calcium, no magnesium; ThermoFisher Scientific), Dulbecco's modified Eagle's medium (DMEM, ThermoFisher Scientific), 2-[4-(2-hydroxyethyl)piperazine-1-yl]ethanesulfonic acid (HEPES, Biomol GmbH), Hanks' balanced salt solution (HBSS), 1-ethyl-3-(3-dimethylaminopropyl)carbodiimide (EDC hydrochloride, Aldrich, crystalline), Roswell Park Memorial 1640 Medium (RPMI 1640, ThermoFisher Scientific), Glucose monohydrate (Applichem), Bodipy 581/591 C11 (ThermoFisher Scientific) and Venetoclax (ABT-100, LKT Labs Incl.) were used as purchased. Bam-7, Betaine, Calcein AM, Cytochalasin D, Dynasore, Filipin, E-64d, Pepstatin A, N-acetyl-cysteine, glutathione (GSH), Liproxstatin-1, phorbol-12-myristate 13-acetate (PMA), Tiron (4,5-dihydroxybenzene-1,3-disulfonic acid disodium salt), ZnSO₄ were purchased from Sigma Aldrich. Caspase-1/4/5 inhibitor Z-YVAD-FMK was purchased from R&D Systems. The solvents ethanol (EtOH, Aldrich, absolute), N,N,-dimethylformamide (DMF, Iris Biotech) and deuterated trichloromethane (CDCl₃, Euriso-top, 99.8 % D) were used without further purification. Dichloromethane (DCM) and methyl-tert-butyl ether (MTBE, Brenntag) were distilled before use. Cell culture media, antibiotics and fetal bovine serum (FBS) were purchased from Life Technologies.

2.2. Preparation of MIL-100(Fe) nanoparticles

For the microwave synthesis of MIL-100(Fe) nanoparticles, iron(III) chloride hexahydrate (2.43 g, 9.00 mmol) and trimesic acid (0.84 g, 4.00 mmol) in 30 ml H₂O was put into a Teflon tube, sealed and placed in the microwave reactor (Microwave: Synthos3000, Anton Paar). The mixture was heated to 130 °C under solvothermal conditions ($p = 2.5$ bar) within 30 seconds, kept at 130 °C for 4 min and 30 s, and the resulting solid was cooled down to room temperature. For purification of the solid, the reaction mixture was centrifuged (Sorvall Evolution RC, Thermo Scientific, 47808 rcf / 20000 rpm, 20 min), the solvent was removed and the pellet was redispersed in EtOH. This cycle was repeated two times and the dispersed solid was allowed to sediment overnight. The supernatant was filtrated three times (filter discs grade: 391; Sartorius Stedim Biotech), yielding MIL-100(Fe) nanoparticles, which are left in the filtrate. The nanoparticles were characterized as described below (see Figure S2-S4 and Figure 1).

2.3. Labeling of MIL-100(Fe) nanoparticles for fluorescence imaging

For fluorescence labeling, 1 mg MIL-100(Fe) nanoparticles were incubated with calcein (final calcein concentration 1 mM) or Atto647N maleimide (final dye concentration 0.01 mg/mL). After incubation for at least 30 min, particles were centrifuged (5 min, 16900 rcf), the supernatant was discarded, and

the pellet of particles was suspended in DOPC liposomes as described below for DOPC liposome coating (Section 2.5).

2.4. Preparation of DOPC liposomes

10 mg (12.7 μmol) 1,2-dioleoyl-*sn*-glycero-3-phosphocholine were dispersed in 10 mL DPBS. The dispersion was extruded 11 times with a mini-extruder (Avanti Polar Lipids, Alabama, USA) equipped with a polycarbonate membrane (0.1 μm ; Whatman, GE Healthcare) that was supported by two polyethylene drain discs (10 mm; Whatman, GE Healthcare). The resulting liposomes were analyzed by DLS (see Figure S1).

2.5. Preparation of DOPC-coated MIL-100(Fe) nanoparticles

1 mg MIL-100(Fe) nanoparticles were dispersed in 200 μL DOPC liposome suspension. 200 μL bi-distilled H_2O was added and the mixture was shaken for 1.5 h (600 rpm; RT). The particles were centrifuged and the resulting pellet was washed (3x) and stored in DPBS. The resulting material was characterized by DLS, XRD, IR, HRTEM, SEM, N_2 sorption and zeta-potential measurements. Fe_2O_3 nanoparticles (as nanopowder) used as a control were treated with the same procedure.

2.6. Preparation of HEPES Buffered Glucose (HBG), simulated body fluid (SBF) and artificial lysosomal fluid (ALF)

HEPES (2.38 g, 10 mmol) and glucose monohydrate (28.95 g, resulting in 5 w% glucose) were dissolved in bi-distilled H_2O (490 mL) and the pH was adjusted to 7.4 by addition of NaOH (approx. 10 mL, 0.5 M). SBF and ALF were prepared according to literature.^[1]

2.7. Cell culture

HeLa, A431 (ECACC), A549, MCF7, MCF10A and THP-1 cells were purchased from ATCC or ECACC, as indicated. All cells except for THP-1 were cultured at 37 °C and 5 % CO_2 in Dulbecco's modified Eagle's medium (DMEM), supplemented with 10 % FBS, 100 U/mL penicillin and 100 $\mu\text{g}/\text{mL}$ streptomycin. THP-1 cells were cultured at 37 °C and 5 % CO_2 in RPMI medium with L-glutamine, supplemented with 10% heat-inactivated FBS, 100 U/mL penicillin, 100 U/mL streptomycin and 1 mM sodium-pyruvate. They were differentiated into macrophages by addition of 100 ng/mL phorbol-12-myristate 13-acetate (PMA) for at least 3 days.

2.8. Metabolic activity assay (MTT)

Standard MTT: HeLa (unless stated otherwise) cells were seeded in 96-well plates at a density of 5.000 cells/well 24 h prior to incubation with the different particle concentrations. Particles diluted in 20 μL DPBS were added to each well and incubated on cells for 72 h at 37 °C and 5 % CO_2 . Medium was then removed and, after washing each well three times with 100 μL Hanks' balanced salt solution (HBSS buffer), 100 μL of MTT solution (3-(4,5-dimethylthiazol-2-yl)-2,5-diphenyltetrazolium bromide in medium; 0.5 mg/mL) were added. After an incubation time of 2 h, unreacted dye and

medium were removed and the 96-well plates were frozen at $-80\text{ }^{\circ}\text{C}$ for at least 30 min. The purple formazan product was then dissolved in 100 μL DMSO (dimethyl sulfoxide) per well and quantified measuring absorbance using a microplate reader (TecanSpectrafluor Plus, Tecan, Switzerland) at 590 nm with background correction at 630 nm. All studies were performed in triplicate. The relative cell viability (%) with respect to control wells treated only with 10 μL DPBS was calculated using Excel as $([A]_{\text{test}}/[A]_{\text{control}}) \times 100\%$.

Additional procedures carried out if stated in the respective experiment:

- medium was changed every 24 h to maintain controlled pH
- medium was adjusted to pH 7.2 by adding 15 μL HCl (1 M) per milliliter medium and incubation over night at $37\text{ }^{\circ}\text{C}$ and 5% CO_2
- 10 μL of a 1 M *Tiron* solution was added after medium exchange (after 24 h particle incubation)
- *Liproxstatin* was stored as 10 mM solution in DMSO. After 1:10 dilution in EtOH, 1 μL was added to 100 μL medium in the 96-well plate.
- Z-YVAD-FMK was stored at 2 mM in 10% DMSO/water solution. 1 μL was added to 100 μL medium in the 96-well plate.
- For inhibition experiments by cysteine and GSH, 1 μL of 100x stock solutions in water was added to 100 μL medium in the 96-well plate.
- Inhibitors (*Dynasore*, *Cytocholasin D*, *Filipin* – see section 2.11) were added at the respective concentration together with Lip-MOF.
- Inhibitors (*Pepstatin A*, *E-64d*) were stored as 1 mM solution in DMSO. After dilution in DPBS, they were added at the respective concentration together with Lip-MOF.
- BCL-2/BAX-modulator *Bam-7* was stored as 500 mM solution in DMSO. After 1:10 dilution in EtOH, 1 μL was added to 100 μL medium in the 96-well plate.
- BCL-2/BAX-modulator *Venetoclax* was stored as 500 μM solution in DMSO. After 1:30 dilution in PBS, 1 μL was added to 100 μL medium in the 96-well plate.
- For control experiments, 10 μL DPBS plus the respective amount of the solvent used for suspension of the drugs were added to the medium.

2.9. Calcein AM viability assay

To determine the cytotoxicity of Lip-MOF on macrophages, differentiated THP-1 cells were seeded and treated with Lip-MOF as described above for metabolic activity assay. 72 h after Lip-MOF incubation, cells were washed twice with PBS and incubated in a 2 μM solution of Calcein AM in PBS for 30 min. Subsequently the Calcein AM solution was removed and the cells were lysed by addition of lysis buffer. Fluorescence of the lysed cells was measured with a microplate reader (TecanSpectrafluor Plus, Tecan, Switzerland) at 489 nm excitation and 535 nm emission.

2.10. Determination of the iron uptake in 24 h

HeLa cells were seeded in 96-well plates (Corning Costar, Sigma-Aldrich, Germany) (5000 cells/well; 100 μ L DMEM) and were incubated 24 h post seeding with 10 μ L Lip-MOF or uncoated MOF dispersion (1 mg/mL in DPBS) per well for 24 h (conditions: 37 $^{\circ}$ C; 5 % CO₂). Medium was removed and the cells were washed with DPBS to remove excess particles. By addition of 30 μ L Trypsin-solution (Thermofisher Scientific) and incubation for 10 min at 37 $^{\circ}$ C, the cells were detached from the wells. 100 μ L DPBS was added and the cells were transferred and combined into a 15 mL conical centrifuge tube. After centrifugation (20 min / 7197 rcf), the supernatant was removed and the cells were analyzed using ICP-OES (12 wells combined).

2.11. Determination of uptake mechanisms by thermal endocytosis inhibition

HeLa cells were seeded in 96-well plates (Corning Costar, Sigma-Aldrich, Germany) (5000 cells/well; 100 μ L DMEM) and were incubated 24 h post seeding with 10 μ L Lip-MOF dispersion (1 mg/mL in DPBS) or 10 μ L bare MIL-100(Fe) nanoparticle dispersion (1 mg/mL in DPBS) per well, respectively (conditions: 37 $^{\circ}$ C; 5 % CO₂). After 30 min, medium was removed (12 +12 wells for Lip-MOF and MOF, respectively) and the cells were washed with DPBS to remove non-internalized particles. By addition of 30 μ L Trypsin-solution and incubation for 10 min at 37 $^{\circ}$ C, the cells were detached from the wells. 100 μ L DPBS was added and the cells were transferred into 15 mL conical centrifuge tubes (wells of same particle type were combined). The well plate was afterwards cooled to 4 $^{\circ}$ C for 30 min and the procedure was repeated at 4 $^{\circ}$ C (12 + 12 wells for Lip-MOF and MOF, respectively). After centrifugation (7197 rcf / 7830 rpm, 20 min), the supernatant was removed and the cells were analyzed by ICP-OES. Experiments were performed in biological triplicates.

2.12. Determination of endocytosis mechanism by addition of endocytosis inhibitors

HeLa cells were seeded in 96-well plates (Corning Costar, Sigma-Aldrich, Germany) (5000 cells/well; 100 μ L DMEM). 24 h post seeding, medium was replaced by *Dynasore* (80 μ M), *Cytochalasin D* (10 μ M) or *Filipin* (1 μ M) containing medium (12 wells each). The cells were incubated for 30 min and 10 μ L Lip-MOF dispersion (1 mg/mL in DPBS) per well was added (conditions: 37 $^{\circ}$ C; 5% CO₂). After 30 min, medium was removed and the cells were washed with DPBS to remove excess particles. By addition of 30 μ L Trypsin-solution and incubation for 10 min at 37 $^{\circ}$ C, the cells were detached from the wells. 100 μ L DPBS was added and the cells were transferred into 15 mL conical centrifuge tubes (wells of same particle type were combined). After centrifugation (7197 rcf / 7830 rpm, 20 min), the supernatant was removed and the cells were analyzed by ICP-OES. Experiments were performed in biological triplicates.

2.13. Determination of MOF degradation kinetics

2 mg of MOF nanoparticles were dissolved in 1.5 ml of 80 mM cysteine solution and incubated for varied amounts of time. After incubation, the solution was centrifuged (16900 rcf) for 5 min and an

absorption spectrum was taken of the supernatant (NanoDrop 2000, Thermofisher). To quantify the kinetics, data were evaluated using Origin9.0 and Matlab2016b. After background correction, the degradation kinetics was extracted from the absorbance signal of trimesic acid between 245-248 nm, or by linear decomposition analysis (LDA) using the start and end spectrum of the titration. LDA was based on the two spectra at 0 min incubation time (which represents 80 mM cysteine solution) and at 75 min incubation (which represents maximum amount of free trimesic acid in solution). Experiments were performed three times in total.

2.14. Western Blot GSDMD

160 000 HeLa cells were seeded into each well of a 6-well plate (Corning Inc.). 24 h after seeding the cells, 50 μ L Lip-MOF of a 2 mg/mL solution were added into 3 wells of the plate. The other three wells were used for the control measurements. At the onset of cell lysis, cells were washed twice with DPBS and frozen at -80 °C. The three wells that were treated equally were pooled for the Western Blot assay. Western Blot was performed according to standard procedures. The GSDMD antibody used was rabbit monoclonal Anti-GSDMD antibody (Abcam, [EPR19829], ab210070). The protein amount was normalized to the entire protein content via the Bradford assay and the final result was normalized to the GSDMD content of the untreated control.

2.15. IL-1 β ELISA

5000 HeLa cells were seeded into each well of a 96-well plate. 24 h after seeding, 10 μ L of a 1mg/mL solution of Lip-MOF was added or, for the control cells, 10 μ L of DPBS to the control wells was added. 72 h after incubation with the MOF nanoparticles, the cell medium was collected and ELISA performed according to the manufacturer's protocol (Human IL-1 β ELISA Kit, Sigma Aldrich, RAB0273). To quantify the amount of cellular IL-1 β , each experiment comprised an additional calibration measuring the absorbance for a given amount of protein. The standard calibration curve (Figure S18A) – defined as mean and standard deviation in absorbance as function of standard protein – was determined from the raw data for three replicas and fitted to a logarithmic function $f(x) = a - b \cdot \ln(x - c)$ using a Levenberg-Marquard algorithm for nonlinear least square fitting. The protein concentration in cell supernatant without (Figure S18B) and with Lip-MOFs was determined numerically from the calibration curve using Matlab2016b. According to Mann-Whitney U test, distributions in absorbance values of the control and Lip-MOF sample are significantly different at the 0.05 level.

2.16. Multivariate Raman data analysis

Hyper-spectral Raman imaging was employed to characterize the chemical composition of organelles, in particular lysosomes, within HeLa cells cultured at pH 7.2 or pH 7.4. The recorded hyper-spectral data cube, *i.e.* data set of Raman spectra as a function of spatial coordinate, was first corrected for cosmic rays, Rayleigh scattering and spurious background. Next, noise reduction within the data set

was obtained using a principle component analysis^[2] and reduction to the first 10 components. Finally, hyper-spectral images of unknown composition were characterized by multivariate analysis based on *k-means* clustering (KMC). KMC is an unsupervised algorithm that groups data into a pre-defined number of clusters k . KMC analysis assigns each spectrum within the hyperspectral data cube H of size $n = P \times X \times Y$, where X , Y are the number of spatial pixels and P the total number of pixels of a recorded spectrum. The partition of n spectra into k ($\leq n$) subsets $\mathcal{S} = \{S_1, S_2, \dots, S_k\}$ is based on the minimization of squared Euclidean distances between the original spectrum s_i to the centroid, *i.e.* mean cluster spectrum^[3]

$$\mathbf{arg\,min} \left(\sum_{i=1}^k \sum_{s_j \in S_i^{(t)}} \|s_j - m_i\|^2 \right) \quad (1)$$

$$m_i^{(t+1)} = \frac{1}{|S_i^{(t)}|} \sum_{s_j \in S_i^{(t)}} s_j \quad (2)$$

First, spectra are randomly assigned to k clusters and their mean spectrum $m_i^{(1)}$ per cluster is computed. KMC examines the distance between each spectrum and the computed cluster centroids and each spectrum is assigned to that cluster with the closest mean. In the next step, the centroids are reevaluated and spectra are newly assigned. In an iterative process, this step is repeated until all spectra are located in the cluster with the nearest centroid, or until the overall sum is minimized.

To investigate the influence of pH on the chemical composition, we recorded Raman images of 10 different cells (5 each in a separate petri dish) for both pH conditions. Data on HeLa cells at pH 7.2 and 7.4 were clustered with 3 respectively 4 clusters depending on the chosen area within the cell (see Figure S16). The clusters describe (i) the surrounding medium, (ii) the cellular membrane, (iii) sub-micron sized organelles and (iv) lipid vesicles, as seen by the averaged cluster spectra (Figure S16). For comparison of both pH values, we determined the mean spectrum including standard deviation over $N = 10$ cluster spectra that represented cellular lipid vesicles (Figure S17a).

$$\mathbf{m}(\lambda) = \frac{1}{N} \sum_{i=1}^N S(\lambda)_i \quad (3)$$

$$\sigma(\lambda) = \sqrt{\frac{1}{N} \sum_{i=1}^N (S(\lambda)_i - \mathbf{m}(\lambda))^2} \quad (4)$$

Both spectra are composed by various chemical components ranging over different kinds of lipids, proteins and sugars. To better visualize the difference between both pH values, we took the difference spectrum $d(\lambda)$ (Supplementary Figure S17b).

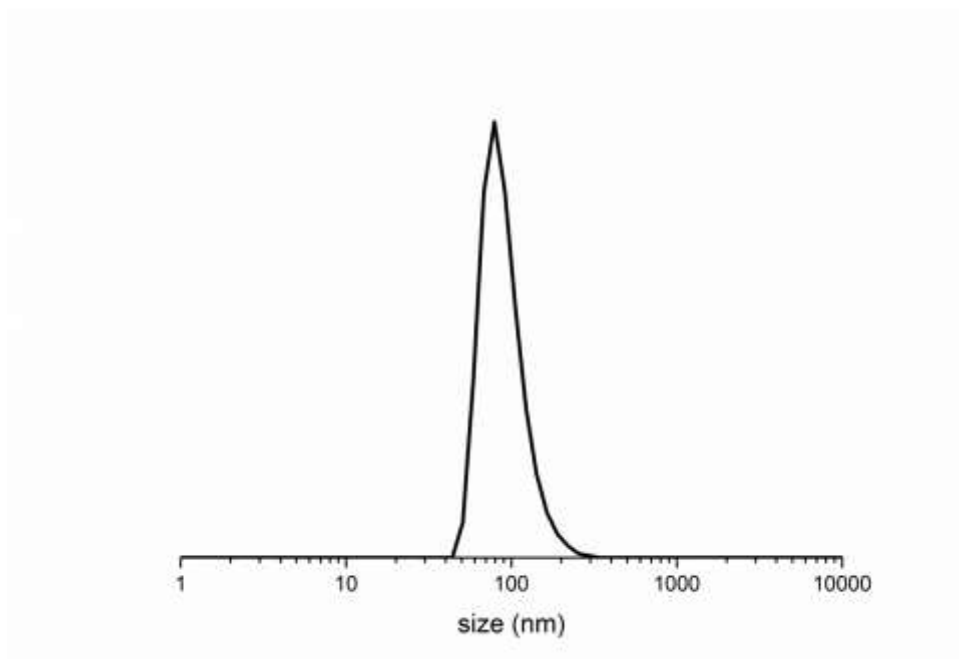
$$\mathbf{d}(\lambda) = \mathbf{m}(\lambda)_{pH\,7.4} - \mathbf{m}(\lambda)_{pH\,7.2} \quad (5)$$

Positive bands describe chemical species that are less abundant at pH 7.2, negative signals refer to chemical species whose concentration has increased. A full list of assigned modes is given in Supplementary Table T1.

All cell experiments of this project were performed in at least biological triplicates and data represent the means and standard deviations. The hyperspectral data was analyzed using WITec Suite FIVE for background correction and cluster analysis. Spectra were processed using OriginPro 9.0 (OriginLab Corp., Northampton, MA, USA).

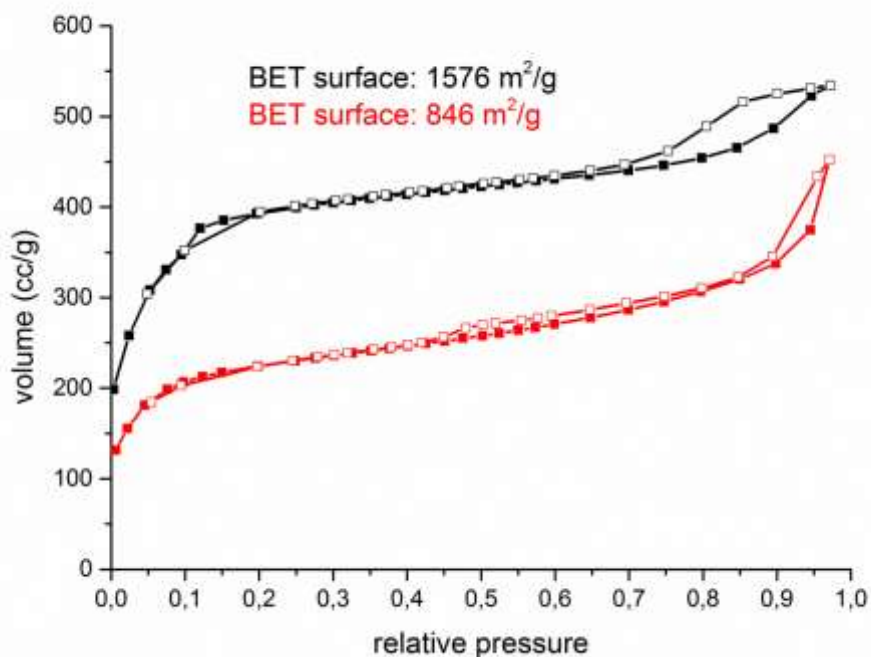
3. *Supplementary Figures*

Supplementary Figure S1



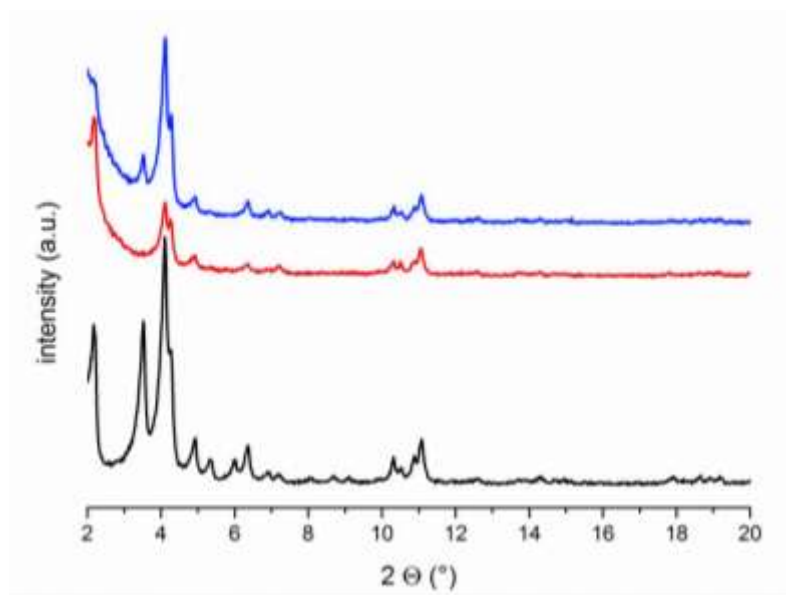
Supplementary Figure S1: Size determination of DOPC-liposomes. DLS measurement of DOPC-liposomes in DPBS buffer solution as used for MOF coating. The measurement shows a size distribution with a peak of about 100 nm as expected.

Supplementary Figure S2



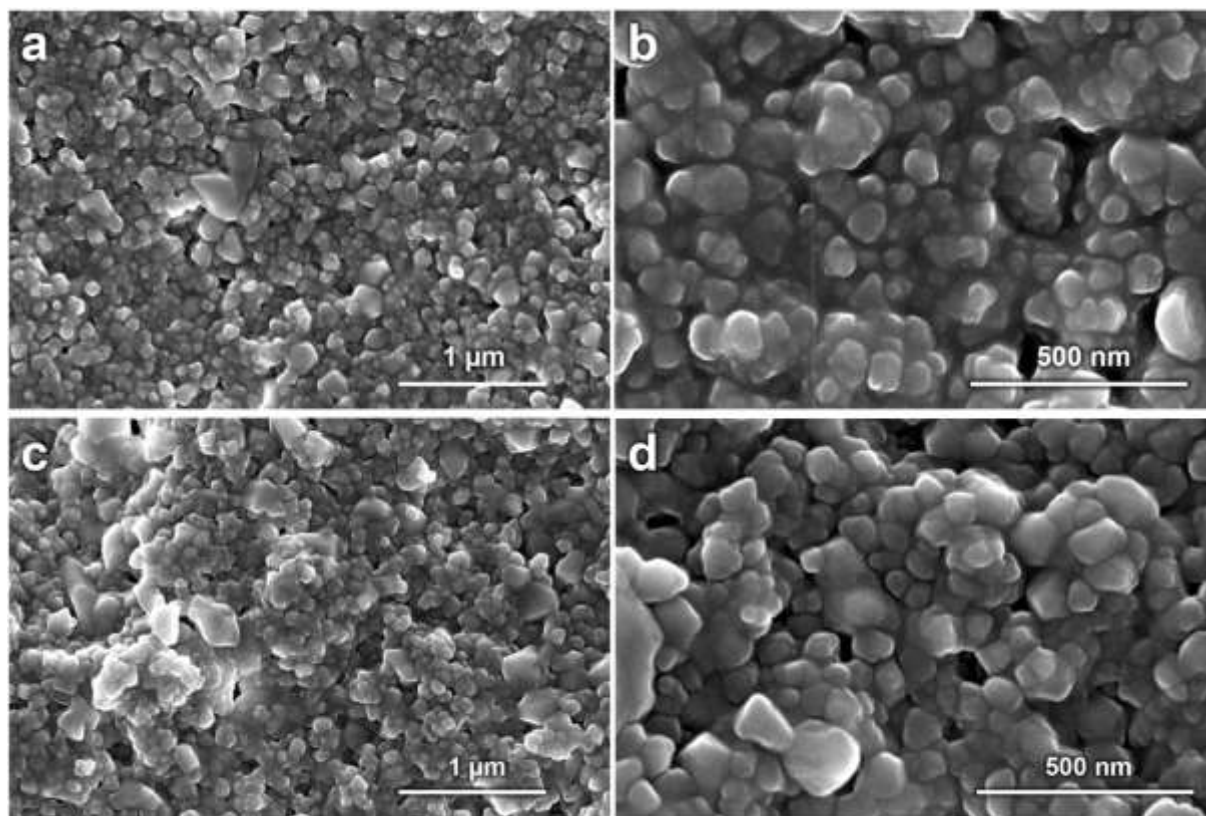
Supplementary Figure S2. Nitrogen sorption characterization. Isotherms of unfunctionalized MIL-100(Fe) nanoparticles (black) and Lip-MOF (red). The BET surface area for MIL-100(Fe) determined from nitrogen sorption fits with reported values^[4]. The decrease in surface area for Lip-MOFs confirms successful lipid-coating. This effect is attributed to the nonporous lipid on the external surface as well as to partial pore blocking.

Supplementary Figure S3



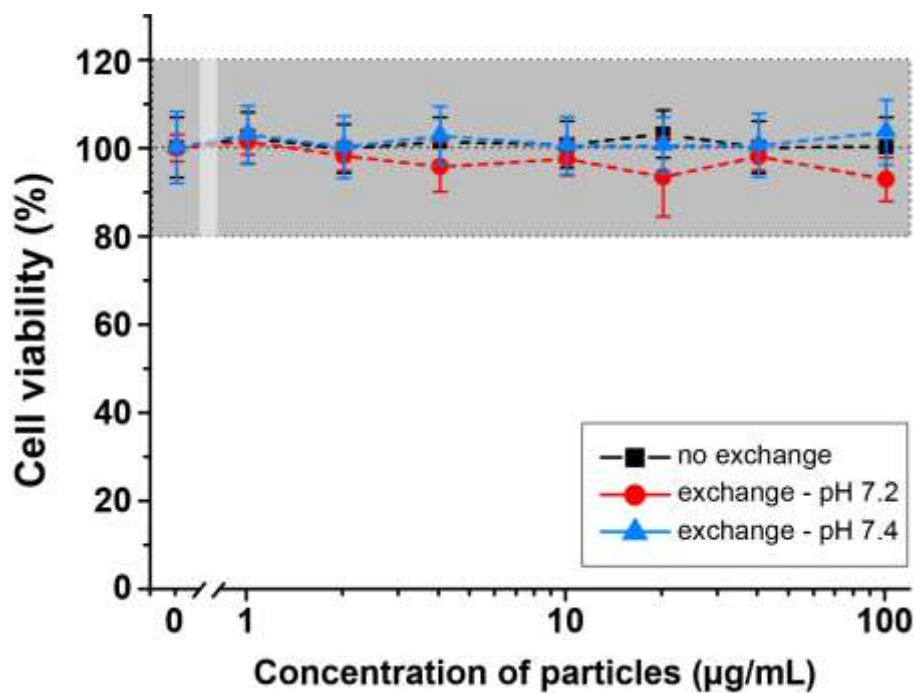
Supplementary Figure S3. XRD characterization. X-ray diffraction patterns of MIL-100(Fe) nanoparticles (black), Lip-MOF nanoparticles (red) and ethanol washed Lip-MOF nanoparticles (blue). MIL-100(Fe) nanoparticles showed characteristic X-ray diffraction reflections as reported previously^[4]. The measurements reveal a decrease in peak intensity (red) after coating due to the high amount of organic material. The intensity can be recovered by washing the particles in ethanol (blue).

Supplementary Figure S4



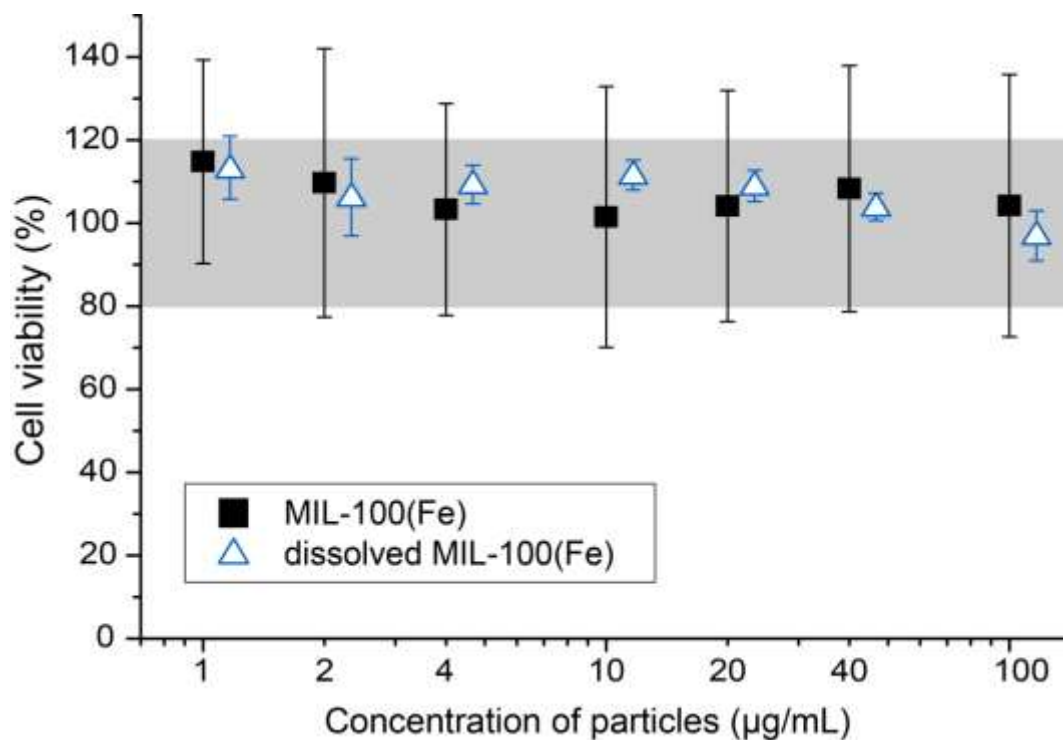
Supplementary Figure S4. Size determination of Lip-MOF via SEM. SEM images of (a-b) uncoated MIL-100(Fe) nanoparticles and (c-d) Lip-MOF at different magnifications (a/c: 50 000 ×; b/d: 150 000 ×). The images show the fairly homogenous shape and size of the nanoparticles. During lipid coating, morphology is maintained.

Supplementary Figure S5



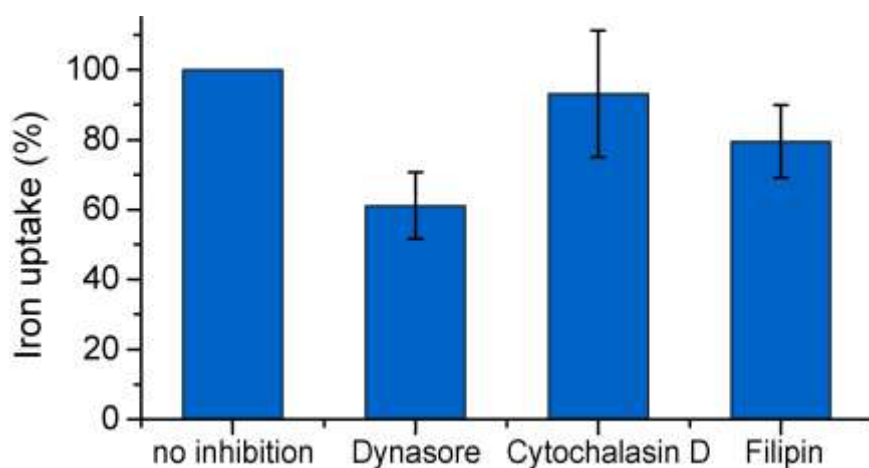
Supplementary Figure S5. Cell viability in the presence of Fe₂O₃ nanoparticles. MTT cell viability assay of Fe₂O₃ nanoparticles under different conditions. Experimental data in black/square: no medium exchange. Experimental data in red/circle: at pH 7.2 with medium exchange every 24 h. Experimental data in blue/triangle: at pH 7.4 with medium exchange every 24 h. Mean values and standard deviations represent the average of triplicates.

Supplementary Figure S6



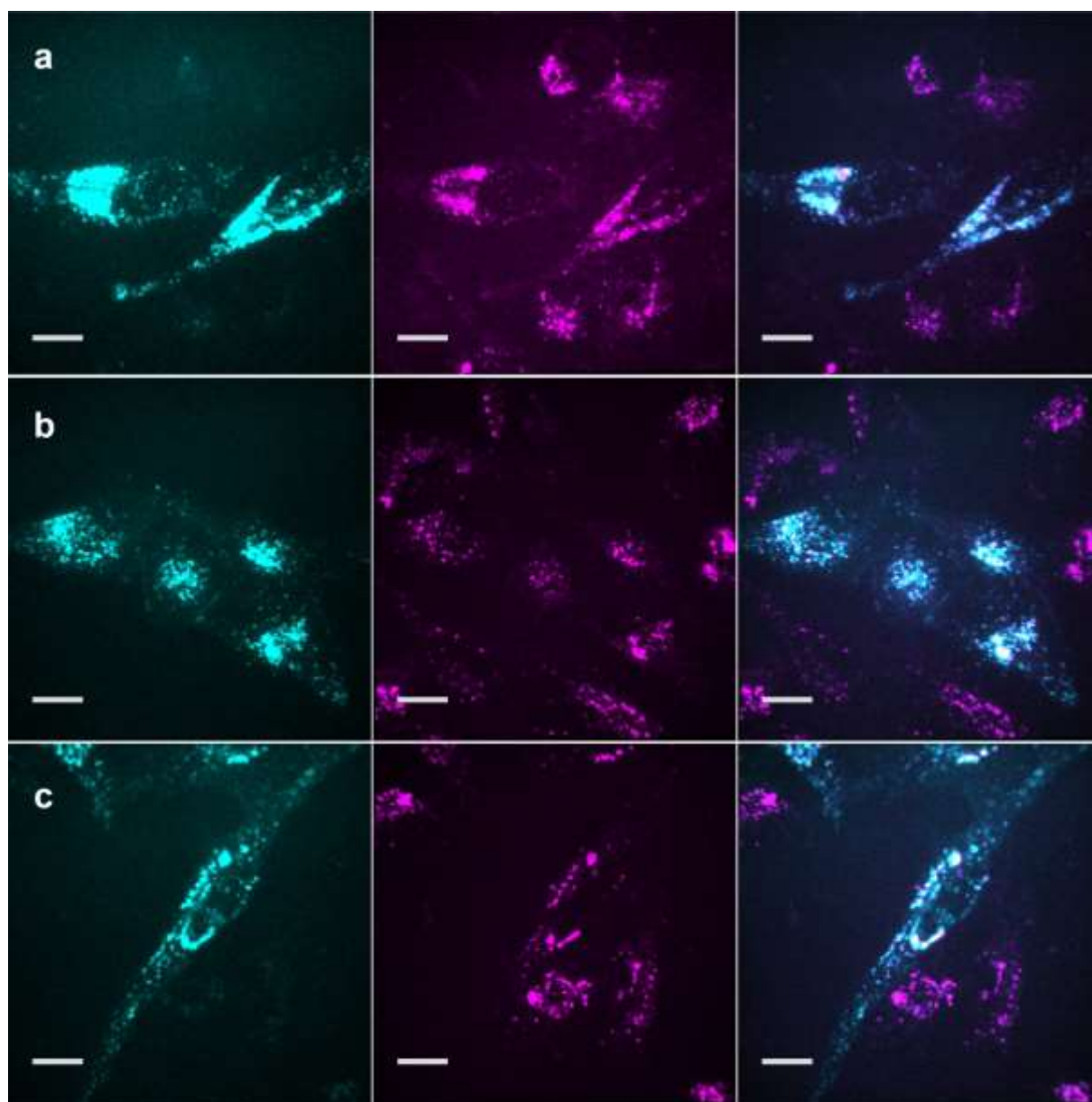
Supplementary Figure S6. Viability in the presence of uncoated MOF particles. MTT cell viability assay of uncoated MIL-100(Fe) nanoparticles (black square) and degraded MIL-100(Fe) nanoparticles (1 mg in 1 mL ALF; blue triangle). Data concerning degraded MIL-100(Fe) nanoparticles shares the same x-axis but was shifted for better visibility. For both conditions, no significant toxicity for the HeLa cells is observed.

Supplementary Figure S7



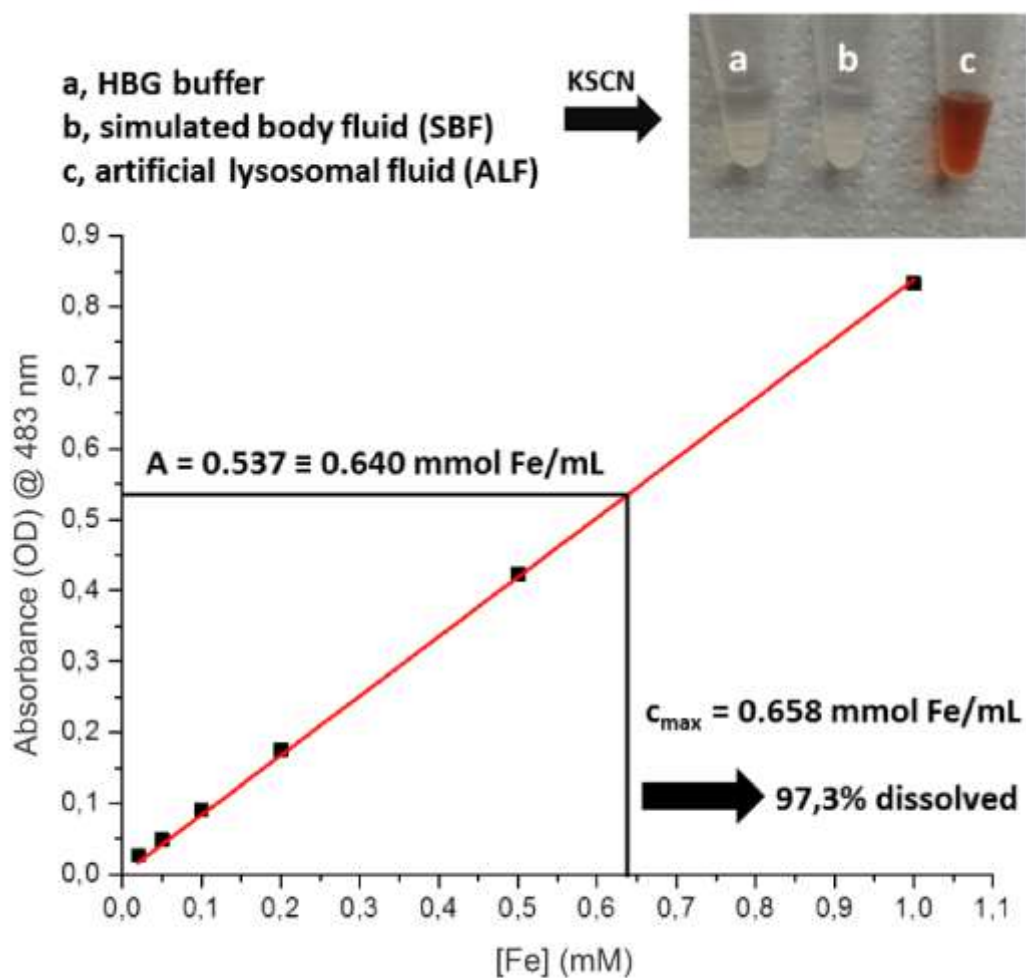
Supplementary Figure S7. Iron uptake. Iron uptake by HeLa cells measured by ICP-OES after incubation for 30 min at 37 °C by addition of different endocytosis inhibitors (80 μ M *Dynasore*, 10 μ M *Cytochalasin D*, 1 μ M *Filipin*). The significant inhibition of Lip-MOF uptake by *Dynasore* suggests clathrin-mediated endocytosis as the main uptake route for Lip-MOF in HeLa cells. *Cytochalasin D* inhibits macropinocytosis and *Filipin* inhibits caveolae-mediated uptake.

Supplementary Figure S8



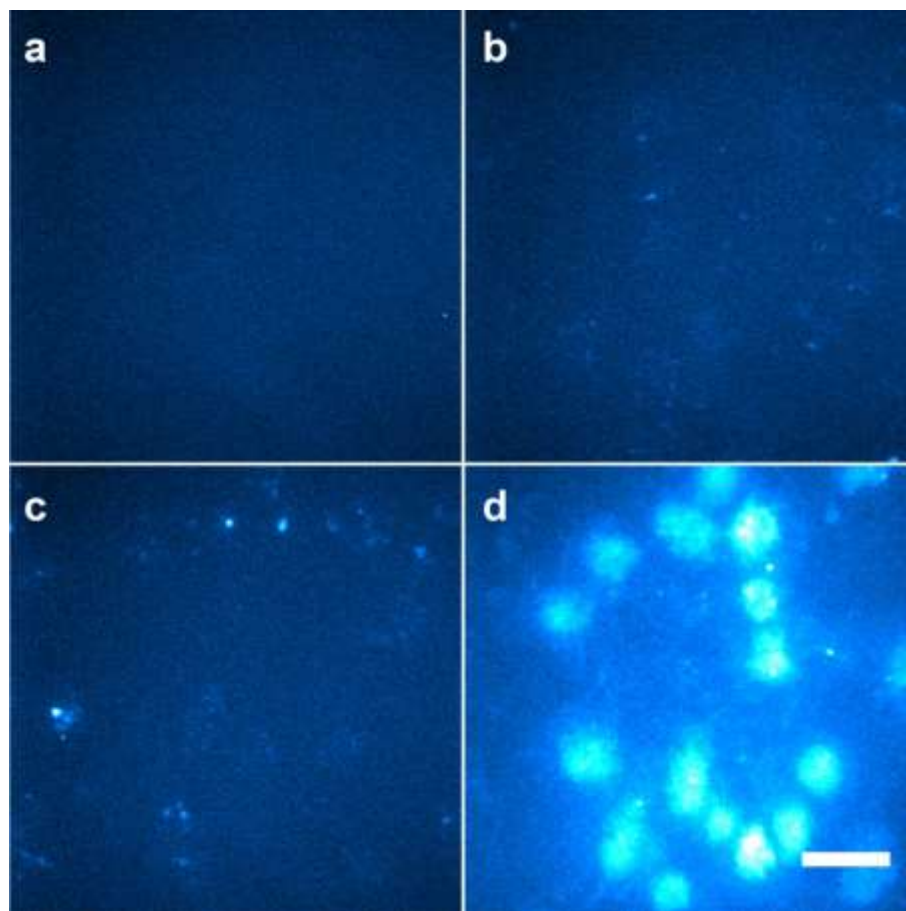
Supplementary Figure S8. Uptake of Lip-MOF in HeLa cells. Confocal microscopy images of HeLa cells incubated with Atto647N loaded Lip-MOF after 40 h incubation without medium exchange. **(a-c)** Examples of different cell measurements. Lysosomes (left; cyan) and nanoparticles (middle; magenta) are co-localized as shown in white in the merged images on the right. Lysosomes were transiently transfected with CellLight Lysosomes-GFP Scale bar: 25 μm .

Supplementary Figure S9



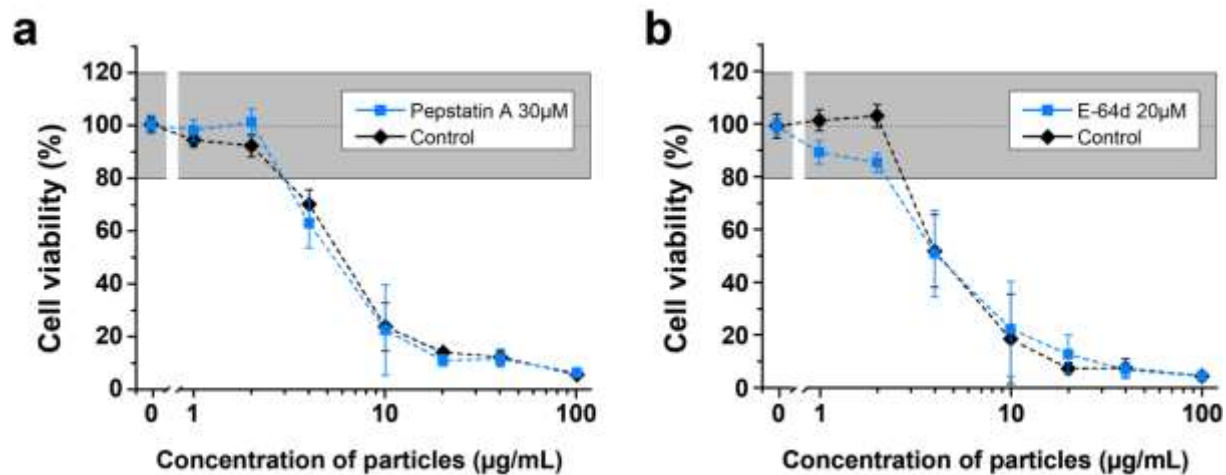
Supplementary Figure S9. Stability test of Lip-MOF over 1h incubation time for different biologically relevant buffers. (Top) A colorimetric assay based on rhodanide indicated no decomposition of the nanoparticles in HBG buffer as well as in SBF. (Bottom) For ALF, the evaluated assay showed an almost complete and rapid decomposition of Lip-MOF.

Supplementary Figure S10



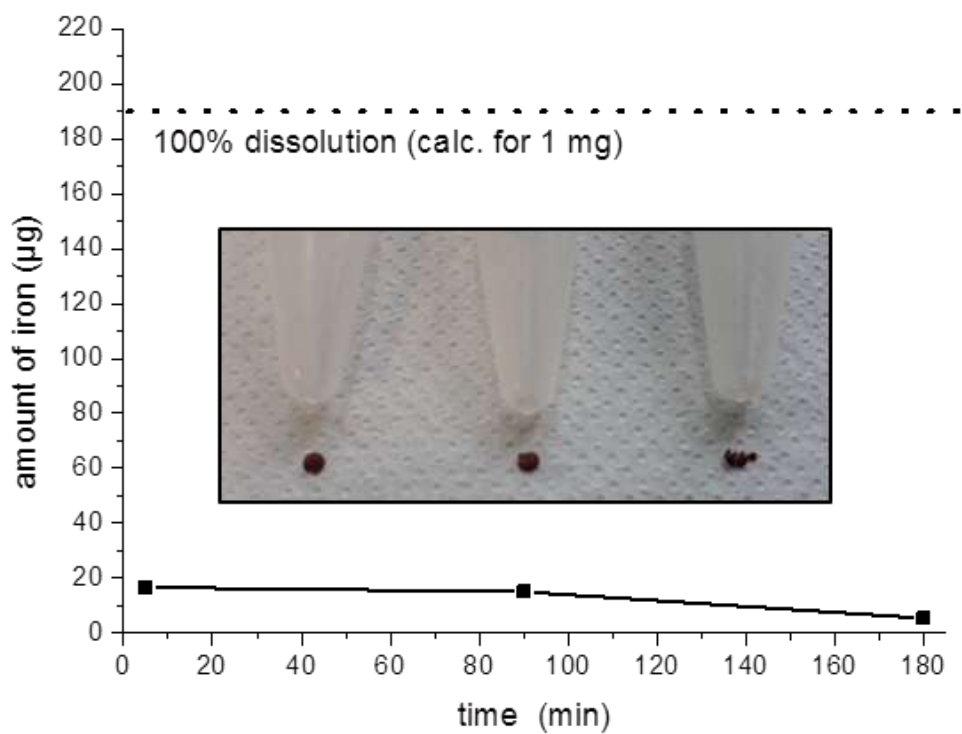
Supplementary Figure S10. Lysosomal calcein-fluorescence in HeLa cells after 48 h incubated under varying conditions. (a) Incubation without Lip-MOFs and medium exchange. (b) Incubation with Lip-MOF at stable pH 7.4. (c) Incubation with Lip-MOF at stable pH 7.2. (d) Incubation with Lip-MOF without medium exchange. Lysosomal degradation of calcein-stained Lip-MOF particles leads to fluorescence unquenching. Images are z-projections of 40 slices with 100 nm separation. Scale bar: 20 μm .

Supplementary Figure S11



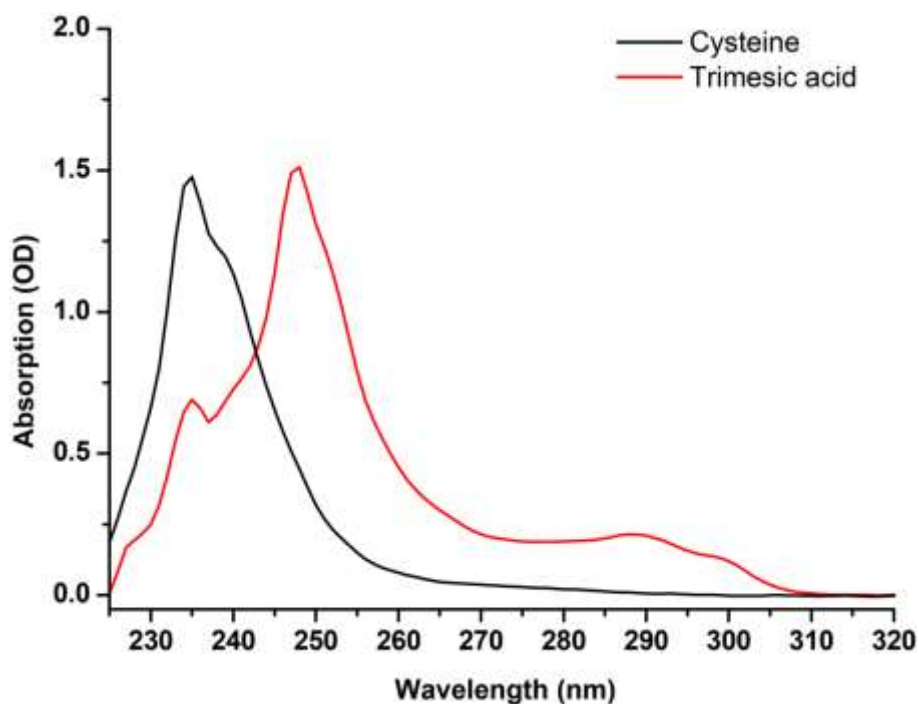
Supplementary Figure S11. MTT cell viability assay on HeLa cells loaded with Lip-MOF in the absence and presence of protease inhibitors. (a) Experiments in the presence of *Pepstatin-A*, which inhibits aspartic proteases such as Cathepsins D and E and Pepsin and **(b)** experiments in the presence of *E-64d*, which inhibits cysteine proteases such as Cathepsin B and L. None of the protease inhibitors influences Lip-MOF induced cell lysis.

Supplementary Figure S12



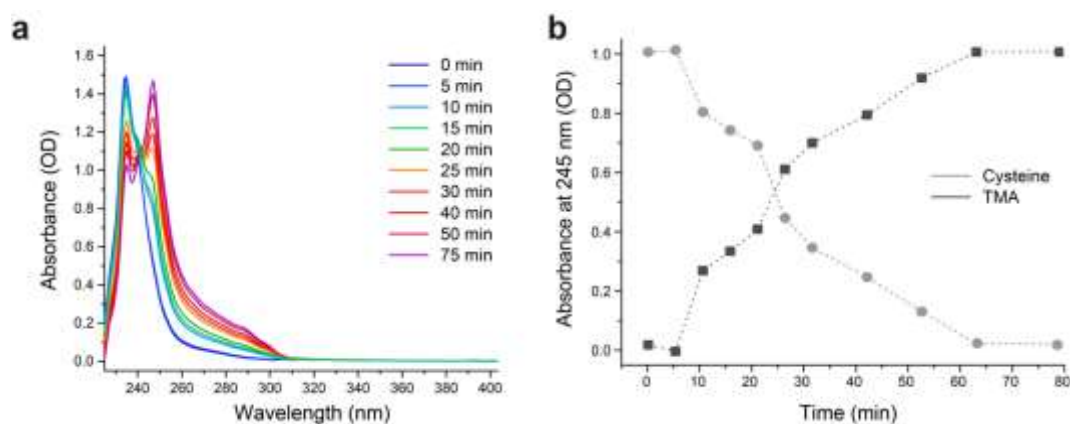
Supplementary Figure S12. Stability in HCl. Dissolution profile of approx. 1 mg MIL-100(Fe) nanoparticles in 0.1 M hydrochloric acid. Iron content was determined by ICP-OES from the supernatant. The inset shows the MOF pellet after centrifugation at the selected time points (5 min, 90 min, 180 min). The dotted line represents the expected amount of iron in the case of full degradation.

Supplementary Figure S13



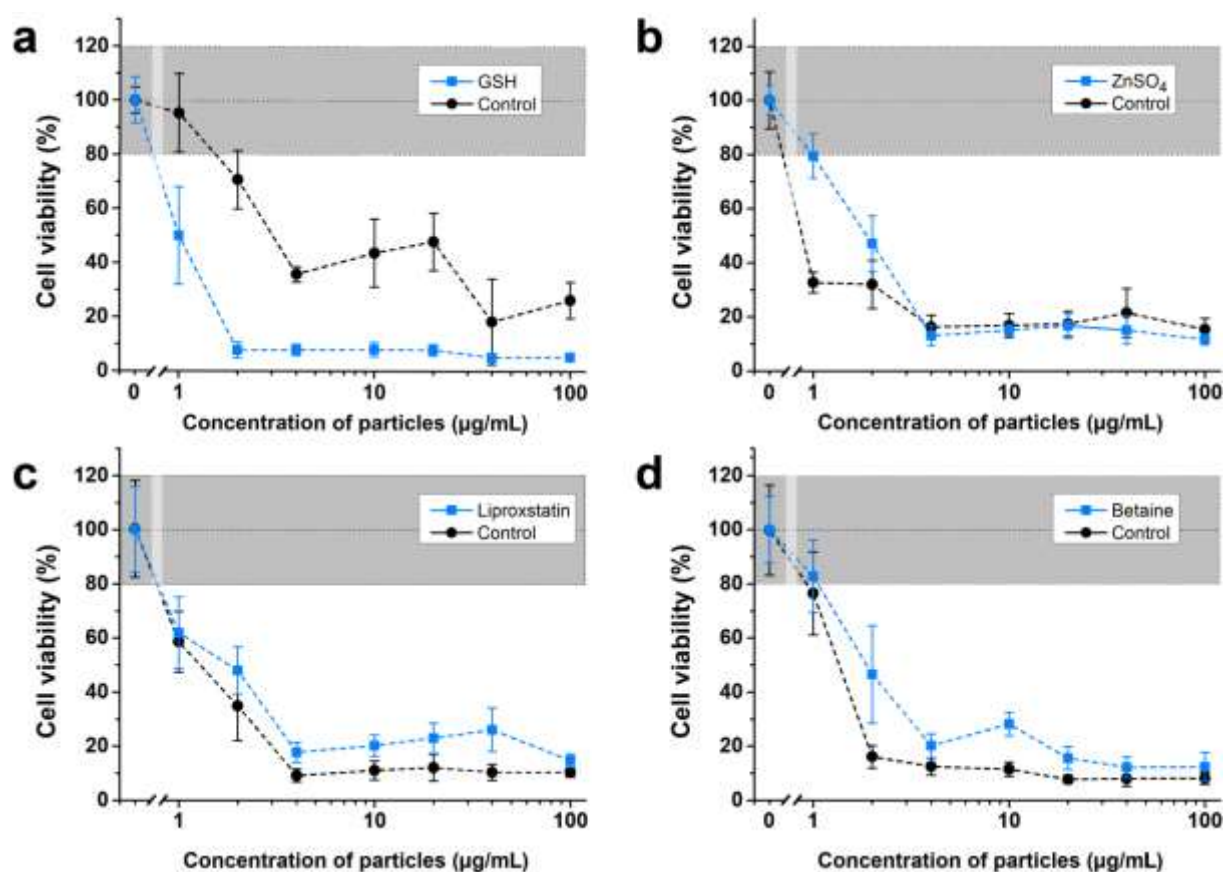
Supplementary Figure S13. UV Absorption of cysteine and Trimesic acid. Absorbance spectra of 80 mM cysteine (black) and a saturated solution of trimesic acid (TMA, red) dissolved in water. While the maximum in absorption for cysteine around 235 nm overlaps with the absorption spectrum of TMA, TMA shows a distinct spectrum with maxima around 248 and 290 nm.

Supplementary Figure S14



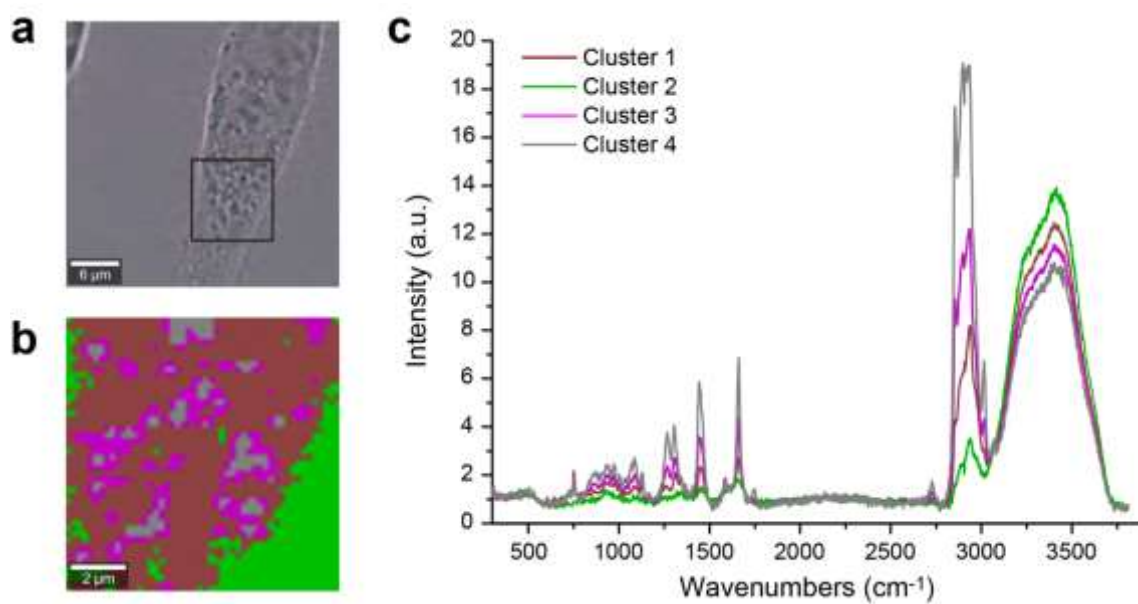
Supplementary Figure S14. MOF degradation in the presence of cysteine. The disassembly of Lip-MOF (2 mg) in the presence of cysteine (80 mM) can either be monitored via the absorbance of trimesic acid around 245 nm as shown in Figure 3 of the main text or by a linear decomposition analysis as shown here for one dataset after baseline correction. **(a)** The spectra obtained using a linear decomposition analysis based on the starting and ending spectrum. **(b)** Reduction of cysteine (starting spectrum) and occurrence of trimesic acid (ending spectrum) are plotted over time.

Supplementary Figure S15



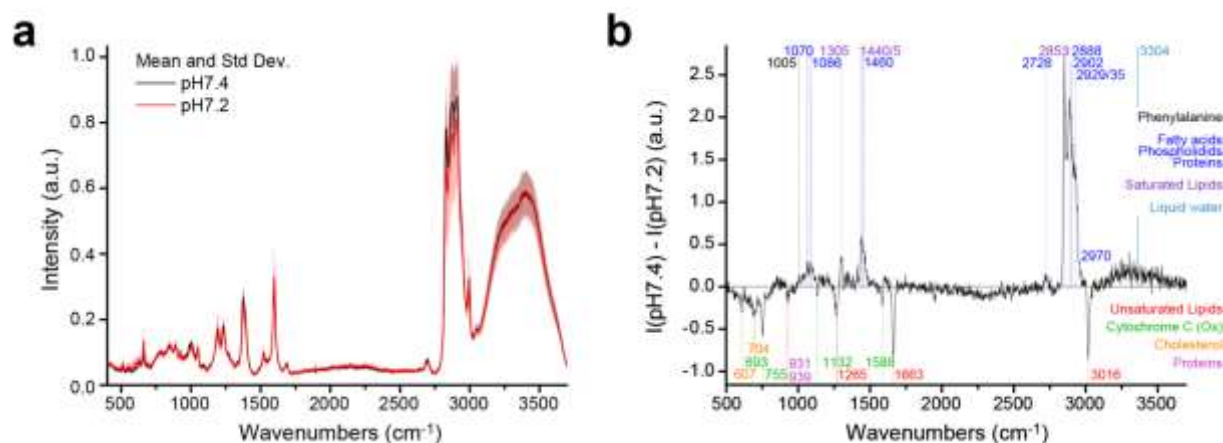
Supplementary Figure S15. MTT viability assay of HeLa cells for varying concentrations of Lip-MOFs in the presence of additional compounds without medium exchange. The viability of HeLa cells as function of nanoparticle concentration is plotted for cells exposed to **(a)** 5 mM GSH in PBS, **(b)** 100 µM ZnSO₄ in PBS (incubated at pH 7.2, no medium exchange afterwards), **(c)** 10 µM *Liproxstatin* –dissolved in EtOH and **(d)** 50 mM Betaine dissolved in water. Mean values and standard deviations represent the average of triplicates.

Supplementary Figure S16



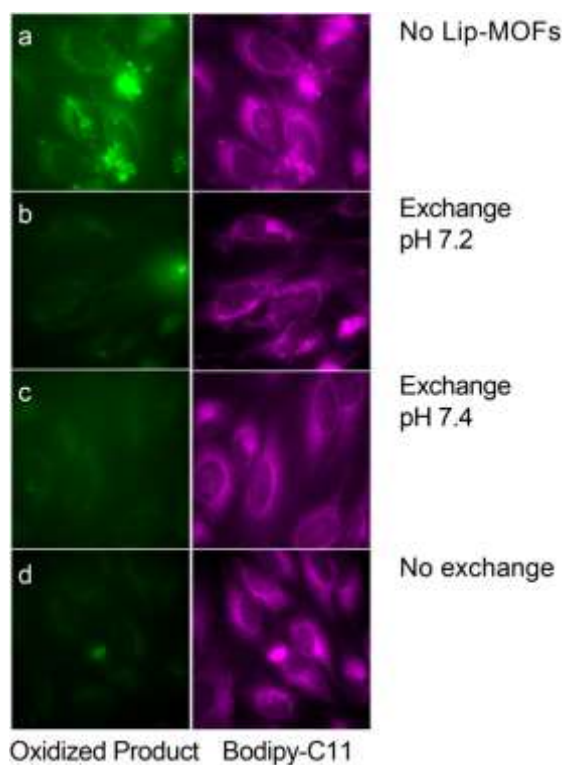
Supplementary Figure S16. Hyperspectral Raman imaging of HeLa cells. (a) Bright field image. (b) Raman image based on *k*-mean clustering with 4 independent clusters. (c) Spectra of the 4 associated clusters. A full list of assigned modes is given in Supplementary Table T1.

Supplementary Figure S17



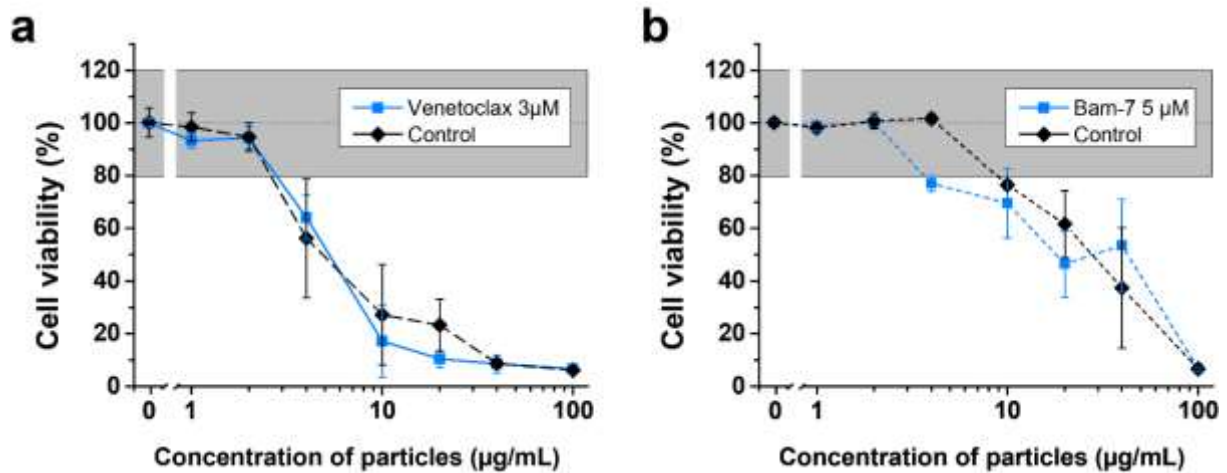
Supplementary Figure S17. Raman signature of lipid vesicles in HeLa cells at pH 7.4 and pH 7.2. (a) Averaged spectrum of lipid vesicles at pH 7.4 (black) and pH 7.2 (red) based on a k mean cluster analysis with 4 clusters. The mean value is derived over 10 independent cell experiments and corresponding cluster analyses. The corresponding standard deviation is shown as the shaded area. (b) Difference spectrum between both pH values. Positive signals refer to chemical species that are more abundant at pH 7.4, negative signals correspond to chemical species that are less abundant. A full list of assigned modes is given in Supplementary Table T1.

Supplementary Figure S19



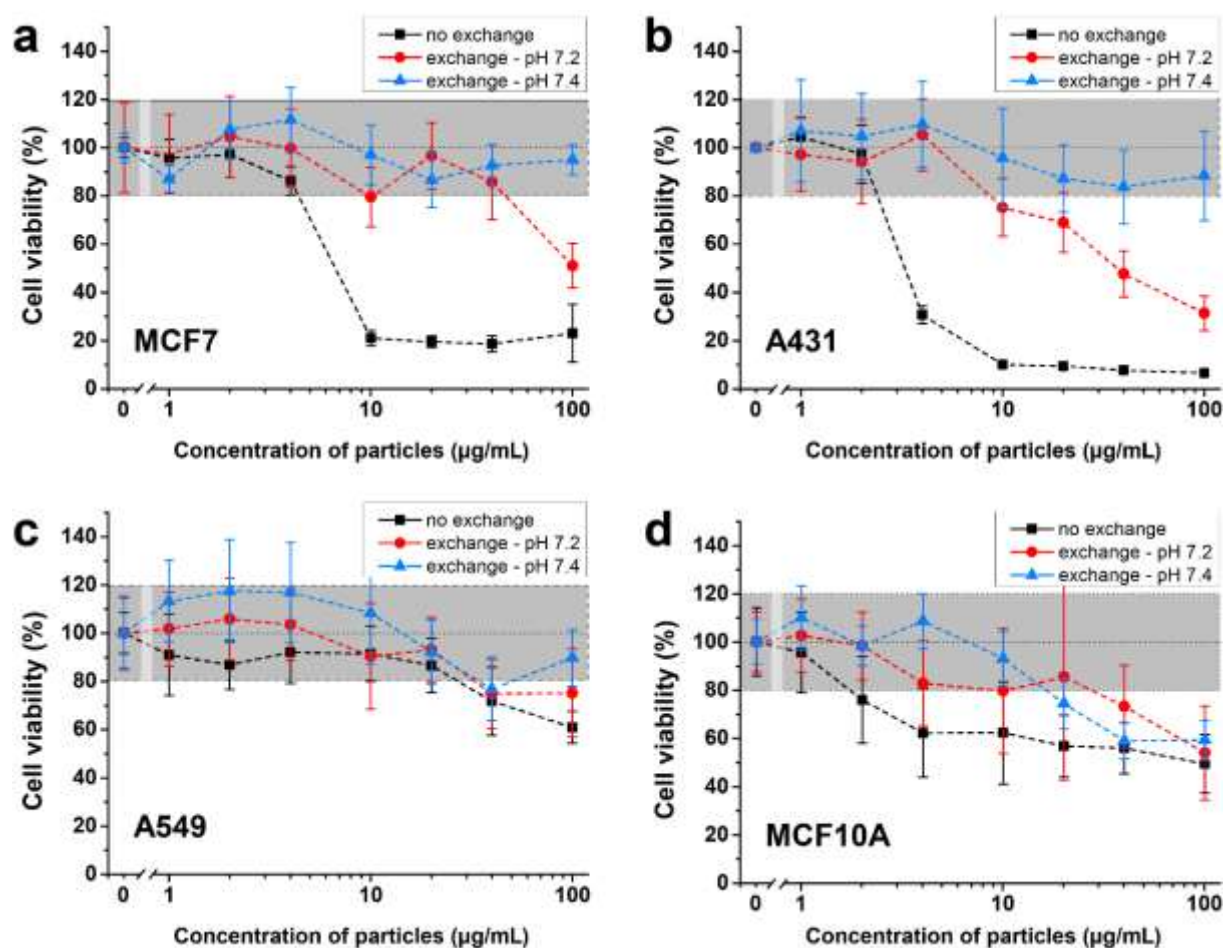
Supplementary Figure S19. Lipid peroxidation monitoring via Bodipy-C11 sensor. Emission of Bodipy-C11 added to HeLa cells without (a) and with (b-d) incubation of Lip-MOF for 48h. Reactive oxygen species due to lipid ROS would shift Bodipy-C11 fluorescence from ca. 590 nm (magenta) to ca. 510 nm (green) and hence lead to an intensity increase in the green channel and signal reduction in the magenta channel. While Bodipy-C11 emission is observed in both detection channels for cells without Lip-MOF, no increase in green emission, *i.e.* no lipid ROS was detected in presence of Lip-MOF particles.

Supplementary Figure S20



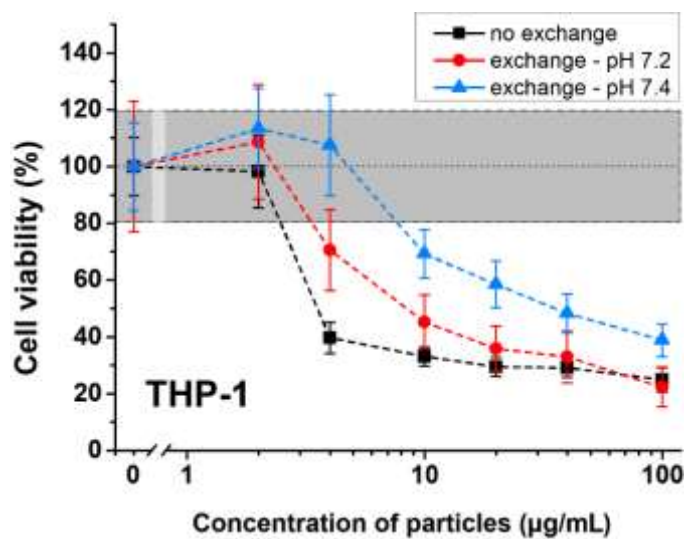
Supplementary Figure S20. MTT viability assay of HeLa cells incubated with Lip-MOFs and BCL family modulating drugs. The viability of HeLa cells as a function of nanoparticle concentration is shown for (a) inhibition of BCL2 by 3 µM *Venetoclax* and (b) activation of BAX by 5 µM *Bam-7*. Both assays show that BCL family proteins are not likely to be involved in the induction of pyroptosis induced by Lip-MOF particles. Mean values and standard deviations represent the average of triplicates.

Supplementary Figure S21



Supplementary Figure S21. MTT viability assay of different human cell lines for varying concentrations of Lip-MOFs at different pH conditions. The viability of cells as a function of nanoparticle concentration is shown for (a) the breast cancer cell line MCF7, (b) the squamous carcinoma cell line A431, (c) the lung carcinoma cell line A549 and (d) the non-tumorigenic breast cell line MCF-10A. **Legend:** Experimental data in black/square: no medium exchange. Experimental data in red/circle: at pH 7.2 with medium exchange every 24 h. Experimental data in blue/triangle: at pH 7.4 with medium exchange every 24 h. Mean values and standard deviations represent the average of triplicates.

Supplementary Figure S22



Supplementary Figure S22. Calcein AM viability assay on THP-1 derived macrophages for varying concentrations of Lip-MOFs for different pH conditions. The used RPMI-medium has less buffer capacity. Thus, daily medium exchange does not keep the pH neutral over the entire time span, which may be a reason for the toxicity observed in this case. **Legend:** Experimental data in black/square: no medium exchange. Experimental data in red/circle: at pH 7.2 with medium exchange every 24 h. Experimental data in blue/triangle: at pH 7.4 with medium exchange every 24 h. Mean values and standard deviations represent the average of triplicates.

4. Supplementary Tables

Supplementary Table T1

ν cm ⁻¹	pH 7.2	pH 7.4	pH 7.2 cm ⁻¹	pH 7.4 cm ⁻¹	Assignment	Chemical species Reference	Reference cm ⁻¹
607			608		Cyto C Cholesterol	Cytochrome C ^[5] Cholesterol ^[6]	605 608
670-690 693			670-690 696		ν (C-S) Cyto C	Cysteines ^[7] Cytochrome C in mitochondria ^[5a]	685 / 693 692
704			707		Ring Cholesterol	Ring deformation Cholesterol (ester) ^[6]	702 / 704
			723	723	$\nu_s(N^+(CH_3)_3)$	Choline ^[6a, 6b]	721
734			734		PS	Phosphatidylserine ^[6c]	733
755			752	752	Cyto C Ox	Cytochrome C ^[5, 6d] Cytochrome C Oxidase ^[8]	752 755
			782	782	Pyrimidine	Ring breathing DNA/RNA ^[6a, 6d]	783
822			822			Phosphodiester ^[6d]	822
854			853	857	Ring Tyr	Ring breathing Tyrosine ^[6d]	854
876				876	$\nu_{AS}(N^+(CH_3)_3)$	Choline ^[6a, 6b, 6d]	875
			897	897		Phosphodiester	893-896
931			929	929	ν (C-C)	Skeletal C-C, α -helix, proteins ^[6d]	932
939			939	942	ν (C-C)	Skeletal C-C, carbohydrates ^[6d]	939
972			975	973	β (CH)/ δ (CCH)	Saturation: C-H-bending ^[6a] Olefinic ^[6d]	973
1005			1008	1008	Ring Phenyl	Phenylalanine ^[6a, 9]	1007/1008
1034			1036	1034	Ring Phenyl	Phenylalanine ^[6a]	1037
1049			1047	1047	ν (C-O)	Glycogen ^[6d]	1047
1070				1070	ν (C-C)	Triglycerides / fatty acids ^[6d]	1070
1080			1080		Phospholipid	ν (C-C) / ν (CO ₃ ²⁻) / ν (PO ₄ ³⁻) ^[6d]	1080
1086				1086	Phospholipid	ν (C-C) / ν (CO ₃ ²⁻) / ν (PO ₄ ³⁻) ^[6d]	1087
1124			1124	1124	ν (C-C) ν (C-N)	Protein / Lipids ^[6d]	1130-1131
1132			1132		Cyto C	Cytochrome C / Heme ^[5]	1127/1132
1150				1150	δ (CH)	Glycogen ^[6d]	1150
1160				1160	ν (C-C) ν (C-N)	Protein	1158
1176				1176	ω (CH) arom	Tyrosine, Cytosine, Phenylalanine ^[6d]	1176
1267			1267	1270	Amide III δ (C=C)	Amide III Triglycerides (fatty acids) ^[6d] Unsaturation: Phospholipids ^[6a, 6b, 10]	1250-1265 1265 1268-1270
1307			1308	1308	τ (CH ₂ / CH ₃)	Twisting CH ₂ / CH ₃ lipid/protein ^[6a, 6b, 6d, 10]	1306-1308
1338				1338	ν (C-C) Phen	Phenylalanine ^[6d]	1339
1342			1342		τ (CH ₂ / CH ₃)	CH deformation: e.g. protein ^[6d]	1342
1413			1405	1410	δ (CH)	CH deformation lipids ^[6d]	1406-9
1445			1445	1445	α (CH ₂ /CH ₃)	Saturation: Scissoring ^[6a, 6b, 9-10]	1445
1460			1460	1460	δ (CH ₂ /CH ₃)	Deformation of lipids	1460
1586			1583 1590	1583 1590	β (C=C) Cyto C ν (C-C)	Phenylalanine (3) ^[11] Cytochrome C ^[5, 6d] olefinic stretch ^[11] Ring Phenylalanine ^[11]	1583 1585 1587 1588
1605			1605	1605	Ring Phenyl δ (C=C)	Phenylalanine ^[6d] Tyrosine, Cytosine ^[6d]	1605 1605
1663			1663	1663	ν (C=C) Amide I	Unsaturation: lipids, fatty acids ^[6, 9] Amide ^[6d]	1661/1662
			1746	1749	ν (C=O)	Phospholipids / Fatty acids / LDs ^[6a-c, 9]	1744/1750
2728			2726	2728	ν_s (NH)	Saturation: Lipids / NH, NH ₃ ⁺ ^[6d]	2727
2853			2858	2855	ν_s (CH ₂)	Saturation: Lipids, proteins ^[6b, 6d]	2855
2888					ν_s (CH ₃) ν_{AS} (CH ₂) ν_s (CH)	Saturation: lipids fatty acid ^[6d] Saturation: alkane chains ^[6a, 6b, 10] Saturation: Protein – CH ^[6b, 6d]	2885 2888-2902 2902
2902			2902	2900			
2929			2929	2929	ν_{AS} (CH ₂)	CH ₂ asymmetric stretch ^[6d]	2929
2935			2935	2935	ν_s (CH ₃)	Saturation: chain end CH ₃ ^[6d]	2935
2970			2970	2970	ν_{AS} (CH ₃)	Saturation: lipids, fatty acids ^[6d]	2970
3016			3016	3016	ν (=C-H)	Unsaturation: lipids ^[6a, 6b, 10]	3012/3015
3200-3600			3200-3600	3200-3600	ν_s (O-H)	Liquid Water ^[6b]	3200-3600

Supplementary Table T1. Raman mode assignment. Nomenclature: α - scissoring; β - bending; δ - deformation; τ - twisting; ν - stretching; ω - wagging. (s - symmetric; as - asymmetric). First column denotes observed frequencies in the difference spectrum (Figure S17b). Columns 2 and 4 named “pH 7.2” denote the presence (red) and wavenumber in the mean cluster spectrum measured at pH 7.2 (Figure S17a). Columns 3 and 5 named “pH 7.4” denote the presence (blue) and precise wavenumber in the mean cluster spectrum measured at pH 7.4 (Figure S17a). The chemical assignment is given in Column 6. The last column (Reference) shows vibrational signatures as reported in literature.

5. References

- [1] M. R. Marques, R. Löbenberg, M. Almukainzi, *Dissolution Technol.* **2011**, 18, 15.
- [2] a) M. G. Ramirez-Elias, J. Alda, F. J. Gonzalez, *Appl. Spectrosc.* **2012**, 66, 650; b) X. Zhang, S. Chen, Z. Ling, X. Zhou, D.-Y. Ding, Y. S. Kim, F. Xu, *Sci. Rep.* **2017**, 7, 39891.
- [3] M. Miljkovic, T. Chernenko, M. J. Romeo, B. Bird, C. Matthaus, M. Diem, *Analyst* **2010**, 135, 2002.
- [4] A. Zimpel, T. Preiß, R. Röder, H. Engelke, M. Ingrisch, M. Peller, J. O. Rädler, E. Wagner, T. Bein, U. Lächelt, S. Wuttke, *Chem. Mater.* **2016**, 28, 3318.
- [5] a) S. Berezhna, H. Wohlrab, P. M. Champion, *Biochemistry* **2003**, 42, 6149; b) N. A. Brazhe, M. Treiman, A. R. Brazhe, N. L. Find, G. V. Maksimov, O. V. Sosnovtseva, *PLOS ONE* **2012**, 7, e41990.
- [6] a) K. Czamara, K. Majzner, A. Selmi, M. Baranska, Y. Ozaki, A. Kaczor, *Sci. Rep.* **2017**, 7, 40889; b) K. Czamara, K. Majzner, M. Z. Pacia, K. Kochan, A. Kaczor, M. Baranska, *J. Raman Spectrosc.* **2015**, 46, 4; c) C. Krafft, L. Neudert, T. Simat, R. Salzer, *Spectrochim. Acta, Part A* **2005**, 61, 1529; d) Z. Movasaghi, S. Rehman, I. U. Rehman, *Applied Spectroscopy Reviews* **2007**, 42, 493.
- [7] a) S. F. Parker, *Chem. Phys.* **2013**, 424, 75; b) A. R. Gargaro, L. D. Barron, L. Hecht, *J. Raman Spectrosc.* **1993**, 24, 91.
- [8] T. Ogura, *Biochim. Biophys. Acta* **2012**, 1817, 575.
- [9] S. F. El-Mashtoly, D. Niedieker, D. Petersen, S. D. Krauss, E. Freier, A. Maghnouj, A. Mosig, S. Hahn, C. Kotting, K. Gerwert, *Biophys. J.* **2014**, 106, 1910.
- [10] K. Majzner, K. Kochan, N. Kachamakova-Trojanowska, E. Maslak, S. Chlopicki, M. Baranska, *Anal. Chem.* **2014**, 86, 6666.
- [11] I. ur Rehman, Z. Movasaghi, S. Rehman, *Vibrational spectroscopy for tissue analysis*, CRC Press, **2012**.